Low Melting Temperature Solder Interconnect Thermal Cycling Performance Enhancement Using Elemental Tuning

[1]Kendra Young, [2,3]Nilesh Badwe, [2]Raiyo Aspandiar, [2]Satyajit Walwadkar, [4]Young-Woo Lee, [4]Hui-Joong Kim, [4]Jung-Tak Moon and [1,5]Tae-Kyu Lee
[1]Portland State University, OR, USA
[2]Intel Corporation, OR, USA
[3]Indian Institute of Technology Kanpur, Kanpur, India
[4]MK Electron Co., Ltd., Yongin, Korea
[5]Cisco Systems, CA, USA
taeklee@cisco.com

ABSTRACT
Recent studies on Sn-Bi based low melting temperature solder interconnects with minor elemental tuning presents enhanced interconnect solder joint thermo-mechanical performance compared to eutectic Sn-Bi. The degradation mechanism towards thermal cycling induced failure is related to twin boundary formation, a different mechanism compared to general Sn-Ag-Cu solder joint interconnect thermal cycling induced degradation. An attempt to slow down the degradation rate is implemented by adding Ag and In into the eutectic Sn-Bi based alloy system. Ag and In contained Sn-Bi solder ball alloy compositions and Sn-Bi based paste with and without Ag content were assembled and the thermal cycling performance compared. In this study, 12x12 mm ball grid array (BGA) components on 62 mil (1.6mm) thick boards were thermally cycled with a -40 to 100ºC profile and 10 min dwells. The correlation between crack initiation, crack propagation, sub-grain development and localized recrystallization were compared with cross section analyses using electron–backscattered diffraction (EBSD) imaging. The analysis revealed the potential thermal cycling performance enhancement mechanism in Sn-Bi solder interconnects.

Key words: Low melting temperature solder, Thermal cycling, Microstructure, EBSD

INTRODUCTION
Sn-Bi eutectic system microstructures are similar to Sn-Pb eutectic microstructure but have different damage accumulation mechanisms, which are less ductile compared to Sn-Pb, where Pb has a face centered cubic crystal lattice. As shown in the Sn-Bi phase diagram in Figure 1(a), the Bi solubility into the Sn varies from 2% to 10%, at room temperature and 100ºC respectively. Unlike the ductile deformation behavior in similar eutectic Sn-Pb systems, the eutectic solder alloy composition of eutectic Sn-Bi exhibits a brittle behavior at elevated temperature conditions [1].

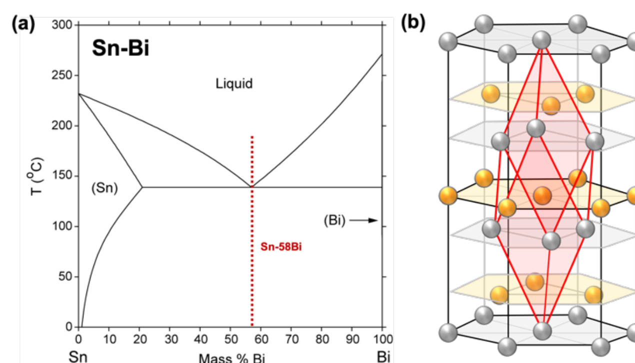

Figure 1. (a) Sn-Bi phase diagram and (b) schematic hexagonal crystal structure of bulk Bismuth (Bi)

Higher Bi solubility induces solid solution hardening inside the solder joint bulk region, somewhat provide strength to the solder joint but triggers brittle behavior at the interface region. As shown in Figure 1(b), the brittle nature of bismuth, is largely attributed to its rhombohedral crystal structure, having two bilayers within its hexagonal structure, and very few of the slip planes that are necessary for material ductility [2]. This characteristic difference is expected to present a different damage accumulation and degradation mechanism compared to Sn-Ag-Cu solder alloy interconnects under thermal cycling, which was explained in earlier studies based on twin boundary formation during thermal cycling. [3,4] While the Sn-Ag-Cu solder interconnects experience a constant development of low angle Sn grain boundaries during thermal cycling, which develops into high angle Sn grain boundaries at localized regions and ultimately into recrystallized grains and crack initiation, the Sn-Bi alloy system interconnects experience a higher solubility of Bi into the Sn region at elevated temperature and a lower solubility at lower temperature at the interface between Sn and Bi rich grains. This cyclic phenomenon during thermal cycling poses a different damage accumulation and degradation mechanism in Sn-Bi system alloy interconnects. As presented in an earlier publication, the Bi solubility increase at higher temperature induced an overall solid solution hardening effect during thermal cycling and once the solder joint reached a saturation in the development of twin boundaries

inside the Sn and Bi grains, the stress concentration point intensity increased at the package side interface and initiated the crack to occur, which is the degradation mechanism in Sn-Bi solder alloy systems. [4] Knowing the potential degradation mechanism in the Sn-Bi system, thermal cycling performance enhancement methods can be considered and implemented. One of the approaches is to utilize micro-alloy elements to delay the Bi diffusion into Sn grains and delay the twin boundary development during thermal cycling. In this study, micro-alloy elements of Ag and In are added either in the solder ball or solder paste and assembled into joint configurations. To compare the potential different behaviors between simple eutectic Sn-Bi system and micro-alloy added Sn-Bi system interconnects, a series of microstructure observations were performed on thermal cycled samples. The microstructural analysis was carried out using Scanning Electron Microscopy (SEM), Optical Polarized imaging, and Electron backscattered diffraction (EBSD) analysis to observe the stress and strain levels associated with the thermal cycling induced damage accumulation per solder ball and solder paste configuration.

EXPERIMENTAL PROCEDURE

To observe the basic deformation behavior of eutectic Sn-Bi system and In added Sn-Bi system, single solder ball shear tests were performed on isothermally aged solder balls as the test set-up, which is presented in Figure 2. Figure 2 shows the 12x12 mm body size ball grid arrays

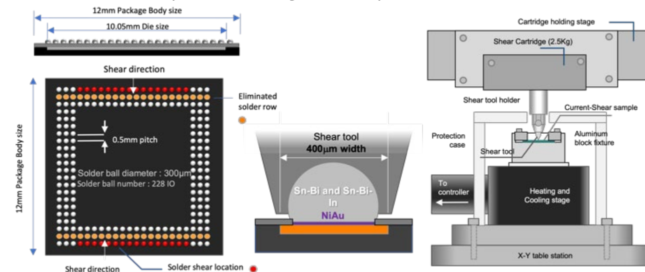

Figure 2. Test vehicle and single solder ball shear test set-up. BGA test component, ball shear tool and solder ball configuration front view and shear tester schematic set-up with heating and cooling stage.[5]

(BGAs) component schematics and the shear test set-up for the BGA. Components have electrolytic NiAu surface finish with a 10.05x10.5 mm dummy die size and the attached solder balls are eutectic Sn-Bi, Sn-Bi-Ag and Sn-Bi-In with 300μm. For the thermal cycling test, the 0.5mm pitch BGA components were assembled on 1.6mm thick 370HR printed circuit boards with Type 4 Sn-Bi and Sn-Bi-Ag solder paste for the Sn-Bi, Sn-Bi-Ag, and Sn-Bi-In ball attached components. The assembled configuration used in this study are as follows: (1) Sn-Bi solder ball + Sn-Bi paste, (2) Sn-Bi-Ag ball + Sn-Bi-Ag paste, and (3) Sn-Bi-In ball + Sn-Bi-Ag paste. The thermal cycling condition for these configuration boards was -40°C to 100°C with 10°C/min heating and cooling rate and 10min dwell times at each temperature extreme. Twelve samples per alloy composition were used for establishing the Weibull plot per the alloy and joint configuration. Cross sectioning for optical microscopy and SEM/EBSD analysis were performed on selected thermally cycled samples. The microstructure analysis was performed using the FEI Sirion XL30 scanning electron microscope (SEM), equipped with an Oxford Instrument High -speed electron backscatter diffraction detector (HS-EBSD). Each EBSD image and data per solder joint was processed with the EBSD software package to get the stress distribution via Grain Reference Orientation Deviation (GROD) maps.

RESULTS AND DISCUSSION

The partially sheared eutectic Sn-Bi solder ball images with room temperature aged and isothermally aged solder balls at 100°C for 500 hours are presented in Figure 3. [5] Compared to the room temperature aged solder ball, the 100°C aged solder ball did not plastically deform much and revealed a crack propagation path at the interface between the solder and pad interface (Figure 3(e) and (h) white boxes).

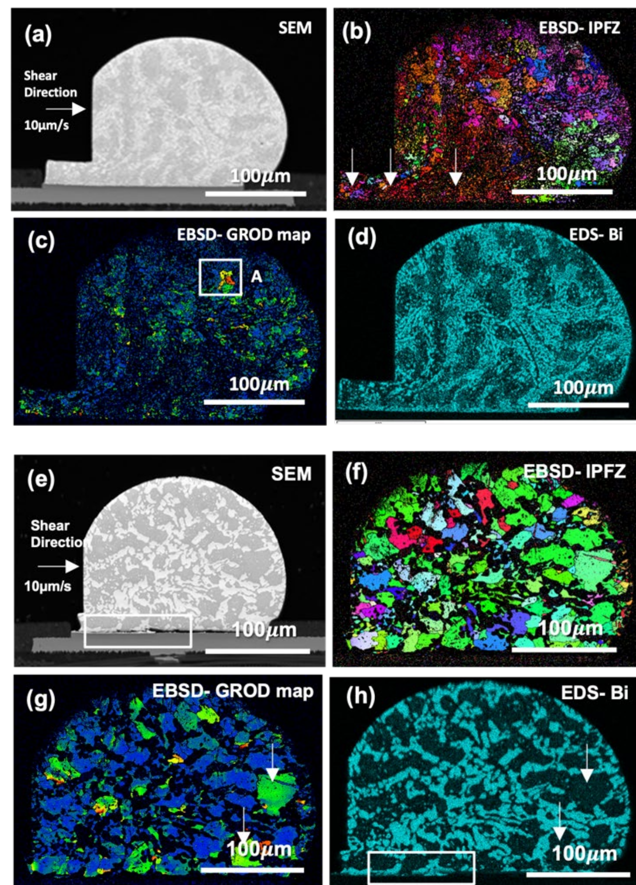

Figure 3. SEM and EBSD cross-section microstructure of partially sheared Sn-Bi solder balls after room temperature aging for 500h (a)-(d), and after 100°C/500h (e)-(h). SEM images (a)(e), EBSD inverse pole figure (IPF) images (b)(f), grain reference orientation deviation (GROD) map (c)(g), and EDS-Bi (d)(h). [5]

Along with the Bi grain growth after aging, the result indicates that the ductility of the solder ball after aging decreased as shown in the associated ball shear measurement

per aging condition for the eutectic Sn-Bi in Figure 4(a)(c) for the room temperature aged solder balls and after 100°C aging in Figure 4(b)(d). Figure 4(a)(b) presents the maximum shear force and Figure 4(c)(d) shows the distance to the maximum peak force, in other words, the ductility per aging condition. As shown in Figure 4(d), the ductility of the Sn-Bi solder ball was low at the initial state and further decreased with further aging at 100°C. Compared to the eutectic Sn-Bi shear test results, Figure 5 presents the shear test measurement with Sn-Bi-In solder balls. As shown in Figure 5(c), the overall distance to maximum shear force indicates a higher ductility from the beginning compared to eutectic Sn-Bi, which was around 80µm for Sn-Bi-In compared to 20µm with Sn-Bi solder balls. The distance to maximum shear force/ductility for 100°C aged solder balls also shows an overall higher value of ductility even though the decreasing trend is the same as Sn-Bi with increasing aging time. This comparison between eutectic Sn-Bi and Sn-Bi-In solder alloy presents and reveals the behavior change the In microalloying effect induces in the Sn-Bi solder joints. The behavior the In microalloying element induces is also expected in thermal cycling performance.

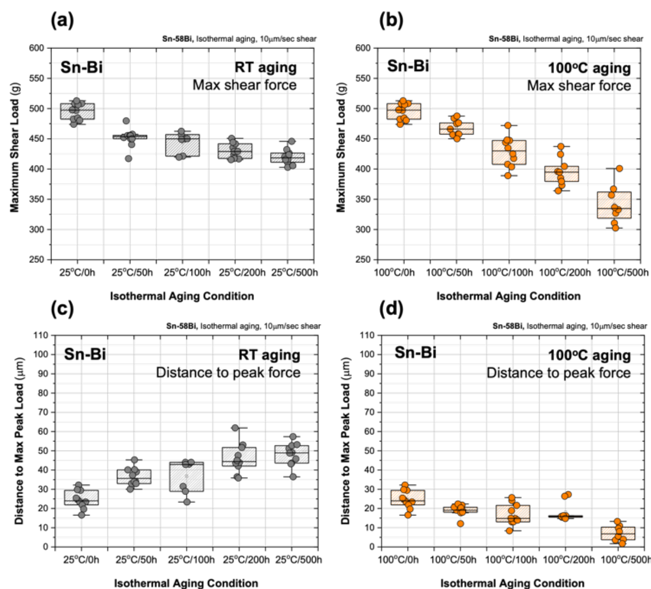

Figure 4. Sn-Bi shear test result. (a)(b) maximum shear force and (c)(d) distance to peak force. (a)(c) room temperature aging and (b)(d) 100°C aging.

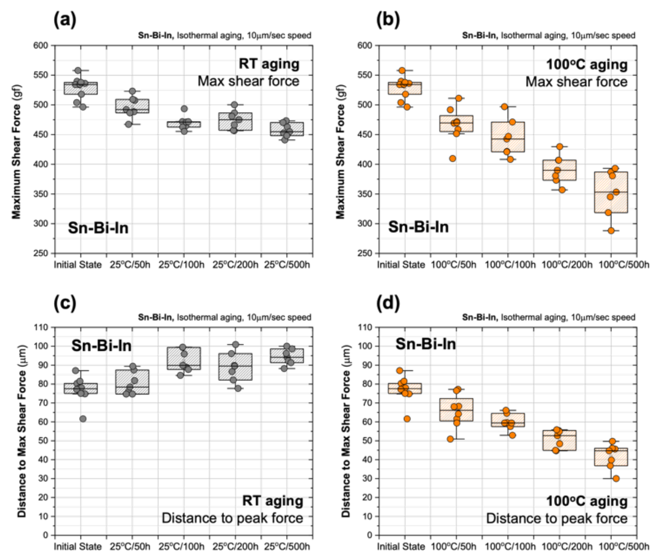

Figure 5. Sn-Bi-In shear test result. (a)(b) maximum shear force and (c)(d) distance to peak force. (a)(c) room temperature aging and (b)(d) 100°C aging.

To identify the impact of the In microalloying effect along with Ag microalloying on thermal cycling, three different joint configurations are tested: (1) Sn-Bi solder ball + Sn-Bi paste (SB+SB), (2) Sn-Bi-Ag ball + Sn-Bi-Ag paste (SBAg+SBAg), and (3) Sn-Bi-In ball + Sn-Bi-Ag paste (SBIn+SBAg). The thermal cycling results per alloy and joint configuration are presented in Figure 6. Figure 6(a) is the Weibull plot along with the failure cycle distribution plot in Figure 6(b). Each box plot in Figure 6(b) indicates the average cycle number to failure and the characteristic life cycle number is listed per condition. As shown in Figure 6(a), the characteristic life cycle number (N63 value) for SB+SB, SBAg+SBAg, and SBIn+SBAg are 2218, 2337, and 3187 cycles, respectively. Compared to the SB+SB and SBAg+SBAg configurations, the SBIn+SBAg thermal cycling performance showed a higher characteristic life cycle and the beta slope (beta slope for SB+SB is 10.4, SBAg+SBAg is 9.6) for SBAg+SBAg (beta slope is 25.4) configuration was steeper than the other two configurations. Since the SBAg+SBAg configuration has Ag in both solder ball and paste, the higher Ag_3Sn precipitates in this joint configuration is expected to play a significant role for the thermal cycling performance.

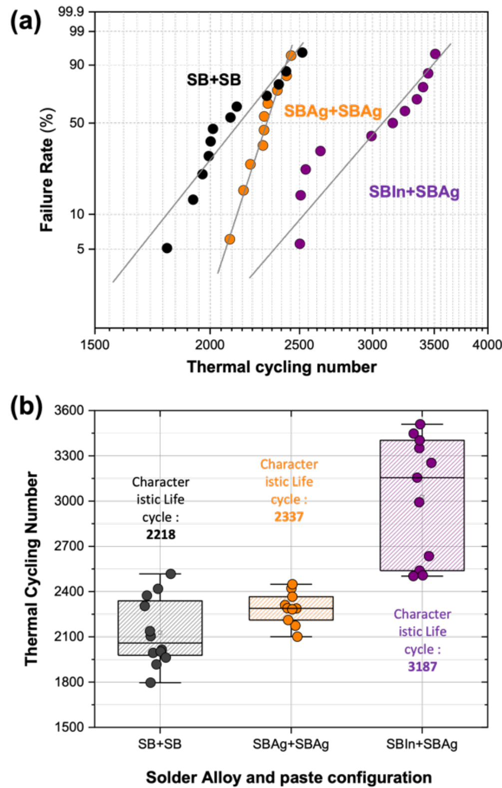

Figure 6. Thermal cycling results. (a) Weibull plots and (b) failure cycle number distribution.

The initial microstructure and the microstructure after crack initiation for both SB+SB and SBIn+SBAg configurations are shown in Figure 7. The EBSD IPF images along with SEM and the EDS-Bi map is presented per configuration. A smaller eutectic grain structure is shown for SBIn+SBAg (Figure 7(c)) compared to the SB+SB configuration in Figure 7(a). A higher magnification SEM image at the SB+SB crack propagation region (Figure 7(b)) is shown in Figure 8.

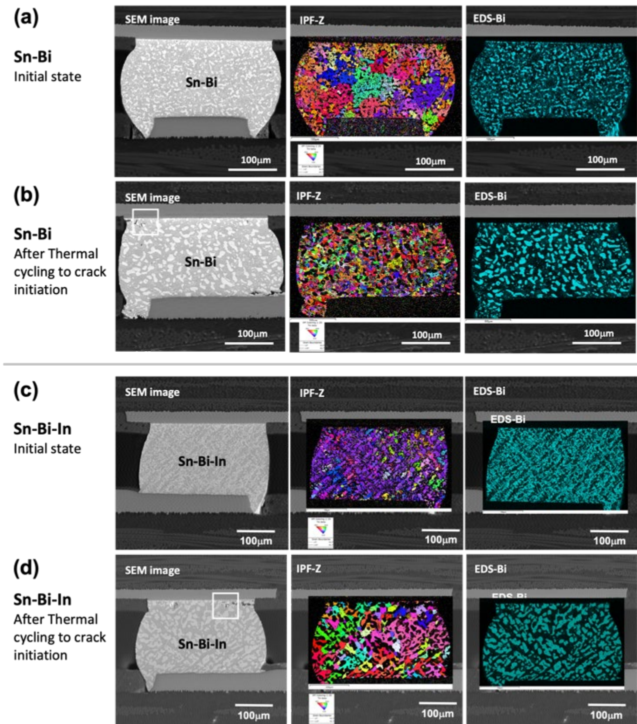

Figure 7. Cross-section SEM, EBSD-IPF and EDS-Bi per (a)(b) Si-Bi and (c)(d) Sn-Bi-In. (a)(c) Initial state and (b)(d) after thermal cycling to crack initiation.

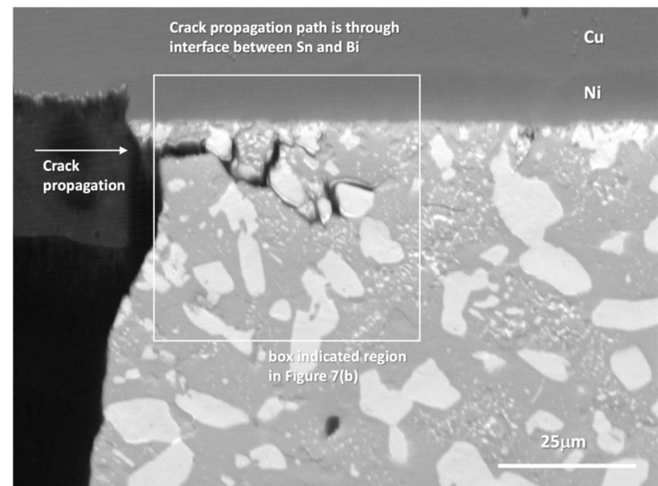

Figure 8. Sn-Bi higher magnification of the indicated white box region in Figure 7(b).

The crack path is between the Sn-rich and Bi-rich grain boundary, which is also observed in earlier studies [3]. As explained in the introduction section, the solubility change of the Bi into the Sn grain region during thermal cycling causes a localized weakness between the Sn and Bi grain boundaries. Compared to the SB+SB crack propagation path, Figure 9 presents the higher magnification crack path in the SBIn+SBAg configuration joint from the region indicated in Figure 7(d). As shown in Figure 9(b) the Bi grain near the crack propagation path shows a sub-grain development as

indicated with a white box. Compared to the fine grained Bi, the neighboring Bi grains do not show the grain refinement and Sn grains show a low phase transformation activity as well, without developing twin boundaries. This means a stress concentration induced grain refinement or sub-grain boundary development is very much localized and not triggered in a wider area.

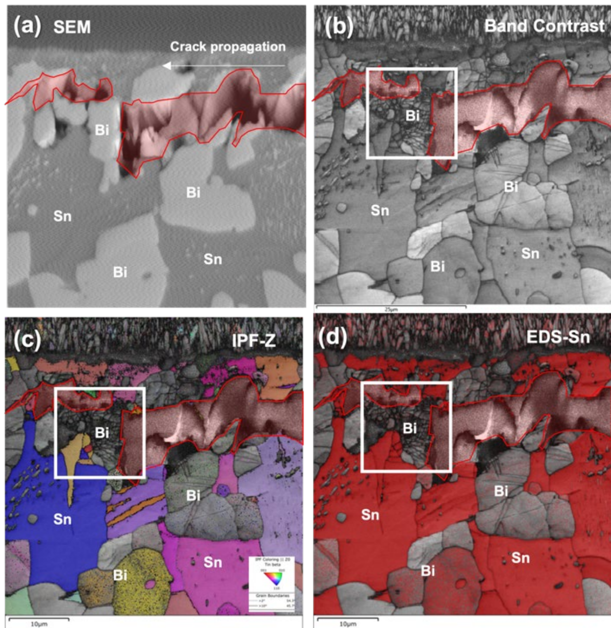

Figure 9. Sn-Bi-In higher magnification of the indicated white box region in Figure 7(d). The white box in (b)(c) and (d) indicates the fine grain sub-grain structure inside the Bi grain.

Published previously, Figure 10 is a Sn-Bi joint with a full crack propagation after 2400 cycles [4]. The associated EBSD-IPF image in Figure 10(b) presents that the Sn-Bi joint damage accumulation near the package side interface is not a localized development of finer grain structure like a Sn-Ag-Cu joint, which contains a degradation mechanism associated with a gradual accumulation of low-angle boundaries in Sn grains which develops into high angle boundaries with crack propagation. Instead in eutectic Sn-Bi, well-developed twin boundaries are observed in the solder joint as indicated by the white arrows, which are also shown in red grain structures in Figure 10(b). But in the SBIn+SBAg configuration presented in Figure 7(d) EBSD-IPF image and Figure 9(c), the twin boundary development is not active as seen in the SB+SB configuration.

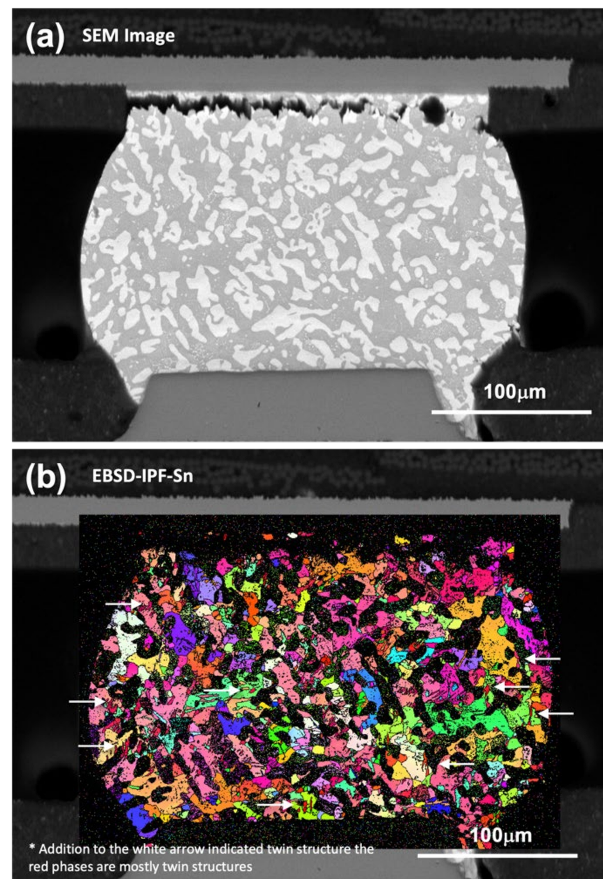

Figure 10. Eutectic Sn-Bi solder joint after thermal cycling to full failure. (a) SEM and (b) EBSD-IPF. White arrows in Figure 10(b) indicates the twin boundaries inside the Sn and Bi grains.

Figure 11 is a larger EBSD-IPF image from Figure 7(d) which does not show active twin boundary development inside the Sn grains compared to the Sn-Bi eutectic solder joint in Figure 10(b).

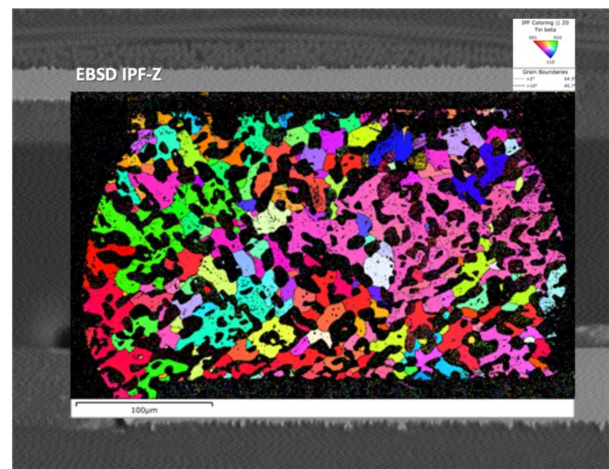

Figure 11. Sn-Bi-In EBSD-IPF image from Figure 7(d).

As shown in the fine sub-grain development in the Bi grain near the crack propagation in Figure 9 white box indicated region, the crack tip region induced a deformation, which

triggered the sub-grain boundary development. The neighboring Bi grains do not show the grain refinement and Sn grains show a low phase transformation activity as well, without developing twin boundaries. This can be explained by the In microalloying in the SBIn+SBAg joint alloy system. Because of the same tetragonal crystal structure and little difference in atomic number between Sn and In element (50 and 49), it is easy for In to replace Sn atoms during the solidification, thus reside inside the Sn as a substitutional atom [6]. It has been reported that In suppresses major Bi grain coarsening after isothermal aging [7,8] and improves elongation, thus ductility [9]. In this study, the observation indicates that the In micro-alloy addition delays the twin boundary development inside the Sn and Bi grain matrix since it mitigates the Bi diffusion into the Sn grain. The In micro-alloy addition also helped improve ductility as observed in the solder ball shear tests results explained above, with and without aging preconditions. Based on the series of observations in thermal cycled SB+SB, SBAg+SBAg, and SBIn+SBAg system soldered interconnects, the damage accumulation and degradation mechanism can be summarized. Localized solid solution hardening occurs at Sn-rich and Bi-rich grain boundaries. The strain absorption capability in the Sn-rich grains reach a limit. Once the limit of the Sn-rich and Bi-rich grains is reached, which cannot further absorb the thermal cycling induced strain, twin boundaries are developed in Sn-rich grains and Bi-rich grains. The localized stress at the package side interface, reaches a stress level for crack initiation. Comparing SB+SB with SBAg+SBAg solder interconnect systems, the Ag micro-alloy contained solder joints somewhat blocks the Bi diffusion into the Sn-grain structure due to the existence at the grain boundaries [10,11] potentially contributes to a higher cycle number to failure. Thus, a higher characteristic life cycle number with the SBAg+SBAg configuration is observed compared to the SB+SB configuration. With In microalloying, the Bi diffusion into the Sn-grain structure is more effectively mitigated, which delays the twin boundary development shown in the EBSD-IPF images, resulting in an even higher characteristic life thermal cycle number, which is observed in the SBIn+SBAg configuration solder joints.

CONCLUSION

The Sn-Bi eutectic system microstructure has different damage accumulation mechanism due to the Bi crystal lattice with a Rhombohedral A7 unit cell structure, which is less ductile and has temperature dependent Bi solubility level into Sn. The nature of the reduced ductility in the Sn-Bi alloy system reveals itself with a different damage accumulation process during thermal cycling compared to Sn-Ag-Cu solder material. Sn-58Bi solder joints show a development of twin boundaries after a certain number of thermal cycles, which help contribute to the stress concentration shift to localized regions, which eventually initiate a crack. Microalloying with In and Ag can mitigate the Bi diffusion into the Sn-grain structure and can delay the twin boundary development thus enabling a higher characteristic thermal life cycle number.

ACKNOWLEDGEMENTS

This work is an outcome of a collaboration project between Intel and the Multi-scale joining and interconnection technology group in Portland State University funded by Intel and the Oregon Metal Initiatives (OMI). The authors thank Greg Baty in Portland State University CEMN for his support on the EBSD analytical work and MK Electron for the material support of eutectic Sn-Bi and Sn-Bi-In solder spheres.

REFERENCES

[1] A. Yamaguchi, Y. Fukuhara, A. Behr, H. Hino, Y. Suzuki and N. Ohashi, The Influence of Resin Coverage on Reliability for Solder Joints Formed by One-Pass Reflow Using Resin Reinforced Low Temperature Solder Paste, IEEE 67th Electronic Components and Technology Conference (ECTC) (2017), pp. 1398-1404.

[2] P. Cucka and C.S. Barrett, The crystal structure of Bi and of solid solutions of Pb, Sn, Sb and Te in Bi. Acta Cryst. 15(1962), p.865.

[3] T.K. Lee, C. Rogan, G. Waduge, Y. Lee, E. Ibe, and K. Loh, Low melting temperature solder interconnect behavior and thermal cycling performance enhancement using edgebond, SMTA International conference and Exhibition proceedings (2020), p.81.

[4] K. Young, R. Aspandiar, N. Badwe, S. Walwadkar, Y. -W. Lee and T. -K. Lee, Thermal cycling induced interconnect stability degradation mechanism in low melting temperature solder joints, IEEE 72nd Electronic Components and Technology Conference (ECTC) (2022), pp.1199-1205.

[5] G.Waduge, G.Baty, Y.Lee, and T.Lee, Isothermal Aging Effect on Sn-58Bi Solder Interconnect Mechanical Shear Stability. J. Electron. Mater. 51, (2022), pp.1169–1179.

[6] Chen, Xu, et al., Effect of In on Microstructure, Thermodynamic Characteristic and Mechanical Properties of Sn–Bi Based Lead-Free Solder. Journal of Alloys and Compounds, vol. 633 (2015), pp. 377–383.

[7] Mokhtari, Omid, and Nishikawa, Hiroshi, Effects of In and Ni Addition on Microstructure of Sn-58Bi Solder Joint, Journal of Electronic Materials, vol. 43(11) (2014), pp. 4158–4170.

[8] Zhou, Shiqi, et al. Improved Mechanical Properties Induced by In and In & Zn Double Additions to Eutectic Sn58Bi Alloy, Journal of Materials Science. Materials in Electronics, vol. 30(8), (2019), pp. 7423–7434.

[9] Mokhtari, Omid, and Nishikawa, Hiroshi, Correlation between Microstructure and Mechanical Properties of Sn–Bi–X Solders, Materials Science & Engineering. A, Structural Materials: Properties, Microstructure and Processing, vol. 651 (2016), pp. 831–839.

[10] Myung, Woo-Ram, et al. Effects of Ag Content on the Reliability of LED Package Component with Sn–Bi–Ag Solder. Journal of Materials Science. Materials in Electronics, vol. 26(11) (2015), pp. 8707–8713.

[11] Hu, F.Q, et al. Influences of Ag Addition to Sn-58Bi Solder on SnBi/Cu Interfacial Reaction. Materials Letters, vol. 214 (2018), pp.142–145.